

MICROCOPY RESOLUTION TEST CHART  
NATIONAL BUREAU OF STANDARDS-1963-A

Unclassified

SECURITY CLASSIFICATION OF THIS PAGE (When Data Entered)



ADA 126123

REPORT DOCUMENTATION PAGE		READ INSTRUCTIONS BEFORE COMPLETING FORM
1. REPORT NUMBER	2. GOVT ACCESSION NO. AD - A126123	3. RECIPIENT'S CATALOG NUMBER
4. TITLE (and Subtitle) WAVE PROPAGATION IN PARTICULATE MEDIA: MULTIPLE SCATTERING OF OPTICAL PULSES IN SCALE MODEL CLOUDS		5. TYPE OF REPORT & PERIOD COVERED Technical Report 9/1/79-8/31/82
7. AUTHOR(s) Richard A. Elliott		6. PERFORMING ORG. REPORT NUMBER
9. PERFORMING ORGANIZATION NAME AND ADDRESS Oregon Graduate Center 19600 N.W. Walker Road Beaverton, Oregon 97006		8. CONTRACT OR GRANT NUMBER(s) N00014-79-C-0897
11. CONTROLLING OFFICE NAME AND ADDRESS Office of Naval Research, Physics Program Office 800 N. Quincy Street Arlington, VA 22217		10. PROGRAM ELEMENT, PROJECT, TASK AREA & WORK UNIT NUMBERS NR394-045
14. MONITORING AGENCY NAME & ADDRESS (if different from Controlling Office)		12. REPORT DATE March 8, 1983
		13. NUMBER OF PAGES 60
		15. SECURITY CLASS. (of this report) Unclassified
		15a. DECLASSIFICATION/DOWNGRADING SCHEDULE
16. DISTRIBUTION STATEMENT (of this Report) Approved for public release; distribution unlimited.		
17. DISTRIBUTION STATEMENT (of the abstract entered in Block 20, if different from Report)		
18. SUPPLEMENTARY NOTES		
19. KEY WORDS (Continue on reverse side if necessary and identify by block number) Optical scattering, pulse delay, pulse stretching, beam spreading, cloud simulation		
20. ABSTRACT (Continue on reverse side if necessary and identify by block number) The results of experiments to measure the delay, temporal stretching, attenuation and spatial spreading of optical pulses in scale model clouds are reported. The model clouds consisted of diiodomethane/water or paraffin oil/water emulsions maintained in a rotating scattering cell to prevent settling of the droplets. The optical pulses were 532 nm, 25 ps duration pulses generated by a frequency doubled, passively mode locked Nd:YAG laser and were detected with a 10 ps resolution streak camera. The measurements of the delay in the mean arrival time of the pulses due to multiple scattering are the first ever measured directly.		

DTIC  
ELECTE  
S MAR 28 1983 D  
E

DTIC FILE COPY

DD FORM 1 JAN 73 1473

EDITION OF 1 NOV 68 IS OBSOLETE  
S/N 0102-LE-014-6601

Unclassified

83 03 28 044

SECURITY CLASSIFICATION OF THIS PAGE (When Data Entered)

WAVE PROPAGATION IN PARTICULATE MEDIA:  
MULTIPLE SCATTERING OF OPTICAL PULSES IN SCALE MODEL CLOUDS

by

Richard A. Elliott

Technical Report

March 8, 1983



<b>Accession For</b>	
NTIS GRA&I	<input checked="" type="checkbox"/>
DTIC TAB	<input type="checkbox"/>
Unannounced	<input type="checkbox"/>
Justification	
By _____	
Distribution/	
Availability Codes	
Dist	Avail and/or Special
A	

Contractor: The Oregon Graduate Center

Sponsor: Office of Naval Research  
800 N. Quincy Street  
Arlington, Virginia 22217

Contract Number: N00014-79-C-00897

Effective Date of Contract: September 1, 1979-August 31, 1982

Principal Investigator: Richard A. Elliott

Reproduction in whole or in part is permitted for any purpose of  
the United States Government.

Approved for Public Release;  
Distribution Unlimited

This manuscript has been submitted for publication  
to Applied Optics.

# MULTIPLE SCATTERING OF OPTICAL PULSES IN SCALE MODEL CLOUDS\*

by

Richard A. Elliott

Oregon Graduate Center

19600 N.W. Walker Road

Beaverton, Oregon 97006

## ABSTRACT

The results of experiments to measure the delay, temporal stretching, attenuation and spatial spreading of optical pulses in scale model clouds are reported. The model clouds consisted of diiodomethane/water or paraffin oil/water emulsions maintained in a rotating scattering cell to prevent settling of the droplets. The optical pulses were 532 nm, 25 ps duration pulses generated by a frequency doubled, passively mode locked Nd:YAG laser and were detected with a 10 ps resolution streak camera. The measurements of the delay in the mean arrival time of the pulses due to multiple scattering are the first ever measured directly.

\*Parts of this work were reported at the Annual Meetings of the Optical Society of America at Kissimmee, Florida October 29, 1981 and Tucson, Arizona, October 21, 1982; at the Conference on Lasers and Electro-Optics, Phoenix, Arizona, April 16, 1982; and at the OSA Topical Meeting on Optical Techniques for Remote Probing of the Atmosphere, Incline Village, Nevada, January 11, 1983.

## MULTIPLE SCATTERING OF OPTICAL PULSES IN SCALE MODEL CLOUDS

### I. Introduction

Multiple scattering by aerosols, dust, and water droplets in clouds or fogs is responsible for a number of deleterious effects which severely impact the performance of imaging, remote sensing, LIDAR and optical communication systems. The work presented here bears some relevance for other systems, but is mainly concerned with the effects of multiple scattering on laser pulse communication systems such as the blue-green satellite to submarine system of interest to the U.S. Navy.

The past decade has seen a considerable effort<sup>1-15</sup> expended on understanding optical pulse propagation in clouds and fog beginning with Bucher's pioneering experiments<sup>1</sup> and Monte Carlo simulations<sup>2</sup> and extending to the recent experiments on the island of Kauai.<sup>4,6</sup> This work has shown the dramatic effects which are possible when multiple scattering and multiple path effects can play a dominant role as occurs in optically thick clouds. Nanosecond duration pulses have been observed to be temporally stretched to more than microsecond duration and theoretical models predict a comparable time delay. An initially collimated laser beam may be spread in spatial extent by an amount approximating the geometrical thickness of the cloud and can have a nearly uniform angular distribution. The only effect which could be said not to be deleterious is the deviation of the

attenuation of the transmitted pulse from the Beer-Lambert law: use of a wide field of view receiver may allow collection of as much as 100 dB more energy than predicted by the single scatter theory.<sup>2</sup>

The current state of understanding as represented by existing theoretical models and scaling laws provides a basis for a good description of the effects of multiple scattering. The available experimental evidence although incomplete does agree reasonably well with these models and serves to lend validity to them.

A common characteristic of most scattering experiments performed in the field on naturally occurring phenomena is the inability to control experimental conditions and the difficulty involved in characterizing the scattering medium. It is not in general possible to adequately instrument the entire propagation path to monitor variations in the medium nor to ensure the reasonable range of conditions necessary to validate a theory. Laboratory experiments thus provide a much needed supplement to the data acquired in field work.

The laboratory system which should logically be used to study scattering in clouds is an artificially generated water droplet cloud since this provides the greatest degree of similarity between the natural and model systems. Such experiments have<sup>16-19</sup> indeed provided very useful information on scattering in optically thin clouds but since the number density of water droplets which can be maintained even under the best conditions is

not much greater than that in atmospheric clouds and the overall dimensions of artificial clouds is on the order of a few meters and an optical thickness of 10 is near the maximum obtainable. In order to study scattering in optically thick media in the laboratory it is a practical necessity to employ other model systems.

A model system should be stable for extended periods and the important scattering parameters subject to some measure of control and be readily characterized. A commonly used system for laboratory studies of Mie scattering, i.e., scattering from particles with diameters comparable to or larger than the wavelength, is a suspension of latex spheres in water.<sup>20</sup> These are generally available in monodisperse size distributions with diameters ranging from tenths to hundreds of micrometers. The quantities needed for multiple scattering experiments involving optical thicknesses in excess of 100 are however prohibitively expensive and moreover only a single index of refraction is accessible.

An alternative to latex spheres is provided by emulsions of dielectric liquids. For, one liquid forms spherical droplets dispersed throughout the other and the optical properties of these systems depend entirely on the liquids used and the size distribution of the dispersed droplets. The size distribution is remarkably stable especially when the emulsion is formed in conjunction with a surfactant and a wide range of refractive indices is available. For this reason all the experiments

reported here were performed on two types of emulsions, either paraffin oil or diiodomethane dispersed in water. The latter system is of special interest since the relative index of refraction of diiodomethane to water is nearly the same as that of water to air and hence is a good model of a cloud.

The mathematical models describing the effects of multiple scattering on pulse propagation give expressions for the pulse stretching, delay, attenuation and beam broadening in terms of the optical thickness, the scattering length and single scatter parameters of the medium. It is possible through the use of an appropriate emulsion to duplicate the single scatter properties of a cloud. The optical thickness is the geometrical thickness divided by the scattering length, which is just the reciprocal of the number density times the average scatter cross section. Thus the optical thickness is directly proportional to number density and use of a dense medium makes it possible to reduce the physical dimensions of even optically thick systems to laboratory scale.

The scattering length or optical mean free path is however inversely proportional to number density. In a dense system then the time interval between scattering events is reduced and faster detectors and shorter duration incident pulses must be employed. For example, 15 ns duration optical pulses are stretched to ~ 10  $\mu$ s duration in clouds a few km thick.<sup>2,4,6</sup> To replicate this situation on a laboratory scale the scattering length must be at

least  $10^3$  times smaller and the detection system must be  $10^3$  times faster. This was achieved in the experiments reported here by using a passively mode-locked Nd:YAG laser frequency doubled to 532 nm as the pulse source and a streak camera capable of 10 ps time resolution as the detector.

## II. Theoretical Models

Mathematical models of the effects of multiple scattering on pulse propagation have been derived from computer simulations and analytic solutions to simplified forms of the equation of radiative transfer.<sup>2,8-15</sup> The physical situation most frequently modelled is that of a cloud layer of thickness  $Z$  in the propagation direction and infinite in extent in the transverse plane.

The Monte Carlo simulations<sup>2</sup> proceed by assuming a ray enters the top of the layer, proceeds a distance  $\lambda_1$ , encounters a scattering center which it leaves in a direction specified by angles  $\theta_1$  and  $\phi_1$  relative to its incident direction, proceeds a distance  $\lambda_2$  and is again scattered. At each scattering a new direction  $(\theta_i, \phi_i)$  relative to its direction before that scattering is specified. The distances between scatterings,  $\lambda_i$ , are distributed exponentially; the azimuthal angles  $\phi_i$  are uniformly distributed between 0 and  $2\pi$ ; and the polar angles  $\theta_i$  are distributed according to the single scatter function,  $P(\theta)$ , appropriate for the size distribution and index of refraction of the particles of the system being modelled.

The ray is propagated in this manner until it exits from the 'cloud' boundary. The path length,  $\sum l_i$ ; the displacement from the axis and angle of exit are recorded and the procedure repeated through many trials. It is then possible to determine the mean and variance of the path length, and the spatial and angular distribution of the exiting rays. Bucher<sup>2</sup> found that the multipath effects in thick clouds could be accurately scaled according to simple equations involving only a few parameters: the optical thickness of the cloud,  $\tau$ ; the mean distance between scatterings,  $b$ ; and the asymmetry factor,  $g$ . These parameters are defined in terms of the geometrical dimensions, number density,  $N$ , and the average single scatter properties of the system as

$$g = 1 - \langle \cos \theta \rangle = 1 - 2\pi \int_0^\pi p(\theta) \cos \theta \sin \theta d\theta; \quad (1)$$

$$b = (N\sigma_s)^{-1} = 2\pi N \int_0^\pi p(\theta) \sin \theta d\theta; \quad (2)$$

$$\tau = Z/b, \quad (3)$$

$Z$  being the geometrical thickness of the layer.

The scaling relations for the mean and standard deviation of the path length according to Bucher<sup>2</sup> are then

$$\langle l \rangle = 0.62 b g^{0.94} \tau^{1.94} \quad (4)$$

$$\text{and } \sigma_l = \langle (l - \langle l \rangle)^2 \rangle = 0.64 b g^{0.81} \tau^{1.81} \quad (5)$$

while the beam radius at which the intensity drops to 0.5 of its on-axis value is

$$r_c = 0.78 b g^{-0.07} \tau^{0.93} \quad (6)$$

and the fraction of the incident light transmitted through the layer

$$I_\tau/I_0 = 1.69 (g\tau + 1.42)^{-1} \quad (7)$$

The delay in the arrival time of an incident delta function pulse and its temporal width are given simply by

$$\begin{aligned} \langle \Delta t \rangle &= \langle l \rangle / c \\ &= 0.62 c^{-1} b g^{0.94} \tau^{1.94} \end{aligned} \quad (8)$$

$$\begin{aligned} \text{and } \sigma_t &= \sigma_l / c \\ &= 0.64 c^{-1} b g^{0.81} \tau^{1.81} \end{aligned} \quad (9)$$

where  $c$  is the speed of light in the medium.

The more recent analytic and computer modelling studies<sup>8-15</sup> have served to confirm these thick cloud results and provided in addition analytic expressions for the pulse shape. In particular Ito and Furutsu<sup>11</sup>, and Ciervo<sup>9</sup> have expressed the temporal behavior as an infinite sum of decaying exponentials of which only the first few terms may be significant under most circumstances. The pulse shape has also been modelled as either a gamma distribution or the sum of two gamma distributions,<sup>6</sup>

$$I(t) = At e^{-at} \quad (10a)$$

$$\text{or } I(t) = A_1 t e^{-\alpha_1 t} + A_2 t e^{-\alpha_2 t}. \quad (10b)$$

Since a completely detailed comparison of pulse shapes is beyond the scope of the present work only the gamma distributions will be referred to below.

### III. Scattering System

#### A. Preparation

The experimental measurements reported here were performed on either of two emulsions: paraffin oil or diiodomethane (DIM) in water. The first was chosen for its ready availability and ease of preparation and handling; the second for its index of refraction, 1.738, which has nearly the same refractive index relative to water as water does to air. The DIM/water emulsion can thus closely simulate the scattering properties of a cloud. In each case lauryl sulphate was used as a surfactant to help stabilize the emulsion.

All materials used may be purchased from chemical supply houses. The DIM ( $\text{CH}_2\text{I}_2$ ) was obtained from two sources, Alpha Products and Aldrich Chemical Co. That supplied by the former was very clear with a faint yellowish tinge characteristic of pure diiodomethane, while that obtained from the latter had been shipped with powdered copper added for stability and had a dark reddish yellow appearance due to the liberation of free iodine. The purity of the DIM was restored by treating it with an aqueous solution of sodium bisulphite followed by anhydrous sodium sulphate to remove any residual water. The absorption coefficient of the purified DIM was measured to be  $\alpha = 2.4 \text{ cm}^{-1}$  at a wavelength of 532 nm. The lauryl sulphate,  $\text{Na}(\text{CH}_2)_{12}\text{HSO}_4$ , was > 99% GC grade manufactured by Fluka, A.G., while the

paraffin oil was purchased from VWR Scientific, Inc. The index of refraction of the oil was measured to be 1.4628 and its absorption coefficient to be  $< 0.0004 \text{ cm}^{-1}$ . All water used including that for cleansing was deionized by a reverse osmosis process and showed a bulk resistivity of  $10^{18} \text{ ohm-cm}$ . The physical properties of the paraffin oil and diiodomethane relevant to this work are listed in Table I.

The emulsions were prepared as follows: 10 ml of oil or DIM in 1 l of 0.5% by weight solution of lauryl sulphate was agitated vigorously, circulated through a stack of three Nuclepore filters (8  $\mu\text{m}$  pore diameter) for several minutes, agglomerations of large drops were removed from the surface by skimming in the case of oil or from the bottom by decanting in the case of DIM. This process produced a coarse emulsion with droplet diameters ranging from  $< 1 \mu\text{m}$  to 50  $\mu\text{m}$ . The location of the peak of the size distribution could be controlled somewhat by varying the rate of flow through the filter stack, a higher flow rate shifting the peak to smaller diameters.

The coarse emulsion prepared in this manner could be stored for periods of days in a slowly rotating ( $\sim 3 \text{ rpm}$ ) cylindrical bottle with horizontally oriented axis until enough had been accumulated for the next stage of preparation.

The coarse emulsions were further refined to produce more nearly monodisperse size distributions by exploiting the differential drift velocity of different sized drops under the influence of gravity. According to Stokes law the steady state

drift velocity of spherical body in a viscous medium is given by

$$V(d) = G d^2 (\rho_o - \rho)/(18\eta) \quad (11)$$

where  $\eta$  is the viscosity of the medium,  $G$  is the acceleration due to gravity,  $d$  the diameter of the sphere, and  $\rho_o$  and  $\rho$  the density of the medium and the sphere respectively. With water as the bulk medium  $\eta = 0.01$  cp and  $\rho_o = 1.0$  while for paraffin oil  $\rho = 0.8755$  and for DIM  $\rho = 3.325$ . Thus a 1  $\mu\text{m}$  diameter oil droplet should rise at  $0.024 \text{ cm hr}^{-1}$ , and a 10  $\mu\text{m}$  diameter droplet at  $2.44 \text{ cm hr}^{-1}$ . On the other hand a 1  $\mu\text{m}$  diameter DIM droplet falls at  $0.46 \text{ cm hr}^{-1}$  and a 10  $\mu\text{m}$  DIM droplet at  $45.6 \text{ cm hr}^{-1}$ .

A separation apparatus consisting of a 20 cm diameter plexiglas cylinder 72 cm long and a hydraulically activated "shutter" located 8 cm from the end as illustrated in Figure 1 was used to selectively remove either large or small droplets. The cylinder with the shutter open was filled with coarse emulsion prepared according to the procedure described earlier and placed in a temperature controlled ( $\pm 0.2^\circ\text{C}$ ) mechanically isolated cabinet to avoid the influence of convection currents and vibration. After a time calculated to allow all oil droplets of a chosen diameter,  $d_c$ , to rise from the bottom past the shutter,

$$T_c = (72-8)/V(d_c) = 1152 \eta/[G|\rho_o - \rho|d_c^2], \quad (12)$$

the shutter was closed. The procedure followed for the DIM systems was essentially the same except then the shutter is

located near the bottom of the column and the droplets fall rather than rise.

The short portion of the cylinder contains all the droplets of the size chosen and greater plus the droplets of smaller size which were already in that volume or which were able to move past the shutter level from regions near it. The longer part of the cylinder contains only droplets smaller than the chosen size. A simple calculation using Eqs.(11) and (12) and the cylinder dimensions gives

$$\begin{aligned} N_L(d) &= N_0(d)[1 - (d/d_c)^2] & ; d < d_c \\ &= 0 & ; d \geq d_c \end{aligned} \quad (13)$$

$$\begin{aligned} N_s(d) &= 1/9 N_0(d)[1 + 8(d/d_c)^2] & ; d < d_c \\ &= N_0(d) & ; d_c \geq d_c \end{aligned} \quad (14)$$

where  $N_0(d)$  is the number of droplets of diameter  $d$  in the coarse emulsion and  $N_L(d)$  and  $N_s(d)$  are respectively the numbers in the longer and shorter lengths of the column after time  $T_c$ .

The emulsion in either length of the cylinder may be collected, made up to its original volume by adding water, stirred to redistribute the droplets uniformly throughout the volume and the process repeated. In this manner it was possible to significantly reduce the variance in droplet diameters. For example, assume the initial size distribution is uniform,  $N_0(d) = N_0$ , and oil droplets with mean diameter near 10  $\mu\text{m}$  are

desired. In this case the time required for a 10  $\mu\text{m}$  diameter droplet to rise from the bottom of the column to the shutter  $T_{10} = 26.23$  hours. If the emulsion which accumulates in the long section of the cylinder is discarded, that which accumulates in the short section retained, diluted to the full volume of the cylinder and the process repeated say four times the resulting distribution will be

$$\begin{aligned} N_1(d) &= N_0 9^{-4} [1 + 8(d/10)^2]^4 ; & d < 10 \\ &= N_0 ; & d \geq 10 \end{aligned} \quad (15)$$

( $d$  in micrometers). If then one final stage to remove the droplets with diameter greater than  $d = 12 \mu\text{m}$  is performed by waiting for a time  $T_{12} = 18.21$  hours and the emulsion in the long section of the cylinder retained, the size distribution which results is

$$\begin{aligned} N_2(d) &= N_1(d) [1 - (d/12)^2] \\ &= N_0 9^{-4} [1 + 8(d/10)^2]^4 [1 - (d/12)^2] ; & d < 5 \\ &= N_0 [1 - (d/12)^2] ; & 10 \leq d < 12 \\ &= 0 ; & d \geq 6 \end{aligned} \quad (16)$$

This has a mean diameter  $\langle d \rangle = 9.32 \mu\text{m}$  and standard deviation  $\sigma_d = 1.30 \mu\text{m}$ .

In practice several factors reduce the effectiveness of the separation process. There is a tendency of particles to coalesce and form larger droplets although this is much reduced by the use of the surfactant, lauryl sulphate. Diiodomethane is slightly

soluble in water and in that case there is a countervailing reduction in droplet size due to gradual dissolution of the DIM droplets. This effect can be minimized by saturating the bulk medium with DIM. Also Stokes law applies strictly only to an isolated sphere. In the high number density systems of interest the movement of one droplet affects those around it so that some cooperative motion results. On the other hand the initial, coarse emulsion does not have a uniform size distribution and the modal diameter can be varied to advantage by means of the flow rate through the Nuclepore filters. Nevertheless, it is possible and practical by the method outlined, to produce systems of droplets which have a desired mean diameter and a standard deviation on the order of 20% of the mean. In the case of oil emulsions a period of about a week may be required but DIM emulsions, because of the greater difference in density and consequent greater drift velocity, may be prepared in the course of a day. Oil emulsion Code F (see Table II and Figure 2) was prepared according to the detailed program outlined above.

#### B. Characterization

A well characterized scattering system is of prime importance if the experimental results are to be of more than limited usefulness. The preparation technique and methods of handling the emulsions used in these experiments were chosen to maintain a stable system whose characteristics varied sufficiently slowly

that continuous monitoring of the system was unnecessary. The emulsions were in all cases thoroughly mixed and kept in the rotating scattering cell described below to minimize agglomeration of the droplets and concentration gradients.

Samples of the emulsion were taken at intervals throughout the course of the optical measurements and the size distribution and number density determined by direct microscopic examination. The emulsion sample was placed in a cylindrical observation cell constructed from a glass microscope slide, a 0.25" I.D. by 0.01" stainless steel washer and a glass cover slip. After the droplets in the emulsion had risen to the cover slip in the case of oil or fallen to the slide in the case of DIM, Polaroid micrographs were taken at 400X. At this magnification and resolution,  $< 1 \mu\text{m}$ , the images were perfect circles indicating that the droplets were actually spherical.

The diameter of each individual droplet on the set of micrographs was measured directly, classed in  $1 \mu\text{m}$  intervals and a histogram of the number in each diameter range constructed. The number density could be calculated from the volume represented by each micrograph and the number of droplets in it. In all cases, several hundred droplets from each sample were measured to provide a reasonable statistical average. The histogram in Figure 2 was constructed in this manner by measuring the diameters of 802 droplets of oil emulsion Code F. This had mean diameter  $9.39 \mu\text{m}$ , standard deviation  $1.69 \mu\text{m}$ , number density  $3 \times 10^{12} \text{ m}^{-3}$ , and volume fraction 0.14%. Also included in Figure 2 is the corresponding theoretical size distribution given

by Eq.16. Note the good agreement between the measured and theoretical mean diameters and standard deviations. Table II lists these quantities, the number density, and the volume fraction of all the emulsions used in the optical experiments.

The single scattering properties of the emulsions were determined by Mie theory from the size distribution and bulk properties of the paraffin oil and diiodomethane. The scatter cross section,  $\sigma_s$ , mean of the cosine of the scattering angle,  $\langle \cos\theta \rangle$ , and the albedo, were calculated for droplets with diameters ranging from 0.1  $\mu\text{m}$  to 30  $\mu\text{m}$  and the average of these quantities weighted by the size distribution histogram determined for each emulsion. The scattering properties of each emulsion are presented in Table III.

#### C. Scattering Cell

The scattering cell is illustrated in Figure 3. A 40 cm diameter by 12 cm cylindrical aluminum tank is suspended in bearings with its axis horizontal and provision made for it to be rotated at a constant speed of about 1 rpm. One end of the tank is closed with a plate glass exit window, the other with an aluminum plate with a 5 cm circular hole in its center through which a sliding hollow tube protrudes. The end of the tube inside the tank is closed with a 2.5 cm diameter glass entrance window and is attached to a 38 cm diameter circular disc which acts as a false tank end. The entire surface of the tank, apart from the windows, is painted flat black to avoid light being reflected back

into the scattering medium once it has 'escaped.' It is thus possible by varying the position of the entrance window and associated false end relative to the exit window to study scattering in a medium bounded by two "infinite" parallel absorbing planes separated by a distance ranging from 2 to 117 mm.

#### D. Optical System

The source of the optical pulses for the delay and stretching measurements was a passively mode-locked Nd:YAG laser which produced a train of around 20 pulses, each 35 ps in duration and carrying  $\sim 100$   $\mu$ J energy. The 1064 nm radiation was double passed through an angle tuned KDP crystal converting approximately 20% of the energy to second harmonic 532 nm light which was separated from the infrared fundamental by a dichroic mirror (see Figure 4). A single green pulse was selected from the train by means of a Pockels cell, the selected pulse being  $\sim 25$  ps in duration.

A portion of the energy of the selected pulse was split off by a beam splitter to trigger the detection system and a further portion split off and routed through a delay line, around the scattering cell, to the detector to provide an accurately timed reference event. The major portion of the selected pulse was directed onto the entrance window of the scattering tank. Provision was made to place neutral density filters in the path of either the reference or primary beam to allow both the reference

and the scattered pulses to be recorded within the dynamic range of the detection system. For all measurements except those on emulsion Code A a Cornu pseudopolarizer was placed in the beam to provide unpolarized incident pulses.

The detector employed in all the pulse measurements was a Hamamatsu Model C979 streak camera capable of resolving events separated in time by less than 10 picoseconds when operated at its fastest streak speed and at lower streak speeds it can display events somewhat longer than 5 nanoseconds. The angular acceptance of the streak camera is approximately cosine squared with a  $36^\circ$  full angle at half-power. One series of measurements on emulsion Code G was made with an aperture restricting the field of view to  $16^\circ$ .

The streak camera provides both analog and digital readout with the actual streak and its intensity profile being displayed on a television monitor. The immediately available record is invaluable in setting up and aligning the experiments. The digital data record is readily stored on magnetic tape for subsequent numerical analysis.

Some spatial beam broadening measurements were made by directing the beam from a cw argon ion laser operating at 514 nm onto the entrance window of the scattering tank. Beam profiles at the exit window were obtained by scanning a pin diode detector along a diameter of the exit window.

#### IV. Experimental Results

##### A. Pulse Stretching, Delay and Attenuation

The pulse scattering experiments were all performed according to the following procedure. After the emulsion was prepared and characterized the scattering cell was filled and placed in the beam as illustrated in Figure 4. The movable entrance window to the cell was positioned at the desired distance from the exit window and a set of approximately 20 intensity versus time records of the reference and scattered pulses were obtained with the streak camera. The digitized events were recorded on magnetic tape for subsequent computer analysis. The entrance window was then repositioned to a different path length and the procedure repeated.

The digitized records of the individual events for each path length were put in precise register by taking the midpoint of the half maximum line of each reference pulse as time zero and summing the 20 individual records. This minimized the effects of pulse to pulse variation and reduced random errors. Figures 5 and 6 are typical examples of these composite records illustrating the dramatic pulse stretching phenomena due to multiple scattering in optically thick media. Figure 5, the results obtained for an optical thickness  $\tau = 9$ , shows the scattered pulse to be only slightly broader than the reference pulse while Figure 6, optical thickness  $\tau = 63$ , shows considerable stretching of the scattered

pulse relative to the reference pulse.

The integrated intensity (area), mean arrival time (centroid), and rms pulse width of both the scattered and reference pulses were calculated from the composite records for each experimental condition. From the integrated intensities, knowledge of the neutral density filters in each path and the corresponding intensities measured in the absence of scattering, i.e., with pure water in the scattering cell, the fraction of the incident intensity which was collected by the receiver could be calculated.

In a similar manner the displacement of the centroid of the scattered pulse from that of the reference could be used to determine the excess delay due to scattering. This entailed taking into account the optical elements, e.g. neutral density filters, in each path, the extra distance the scattered pulse had to travel through water at the longer paths and the amount of delay introduced deliberately in the delay line to position the two pulses a convenient distance apart on the streak record. It may be noted that the delay measurements reported here are the first ever measured. Prior experiments<sup>1,3,4,6</sup> have not been able to determine delays precisely because of the lack of an adequately timed reference signal.

The pulse stretching caused by multiple scattering was calculated by subtracting the second moment of the reference pulse from that of the scattered pulse, taking the square root and

doubling. Twice the rms width,  $2 \sigma_t$ , was chosen for comparison purposes since it is closer to the FWHM of a pulse. For example the FWHM of a gaussian pulse is  $2.35 \sigma_t$  while that of a  $te^{-at}$  shaped pulse, is  $1.73 \sigma_t$ .

The delay time,  $\Delta t$ ; pulse stretching,  $2 \sigma_t$ ; and the ratio of the received intensity to the incident intensity determined in the manner described for each path length (optical thickness) and for all of the emulsions listed in Tables II and III are presented in Tables IVA through IVG. Also, the delay time results are plotted in Figures 7 and 8, the pulse stretching results in Figures 9 and 10, and the relative intensity results in Figures 11 and 12. In order to facilitate intercomparison of the results the delay and pulse stretching measurements have been normalized by multiplying them by  $c b^{-1} g^{-0.94}/0.62$  and  $c b^{-1} g^{-0.81}/1.28$  respectively with the values of  $b$  and  $g$  used being those appropriate to the particular emulsion. Theoretically, according to Eqs.(8) and (9), the data should then fall on the lines  $\tau^{1.94}$  in the case of the delay measurements and on the line  $\tau^{1.81}$  for the pulse stretching measurements. Again for the purpose of ease of comparison the relative intensities are plotted against  $g\tau$  since according to Eq.(7) the points should lie along  $1.69/(g\tau + 1.42)$ .

#### B. Field of View Effect

A series of pulse scattering measurements was also made with the field of view of the streak camera restricted to  $16^\circ$  full

angle rather than its unrestricted field of view of  $36^\circ$ . These measurements were made in the same way as described above but on only one emulsion, Code G. The delay, pulse stretching and relative intensity determined for four optical thicknesses are displayed in Table V and are also plotted as the triangular points in Figures 8, 10 and 12 respectively. These should be compared directly with those results for the same optical thicknesses in Table IVG and the corresponding diamond shaped points plotted in Figures 8, 10, and 12.

### C. Beam Spreading

The irradiance profile at the exit window of the scattering cell was measured by scanning a wide field of view ( $> 120^\circ$ ) pin photodiode across the front of the cell. The profiles obtained when the entrance window was 1, 4, 6, 8 and 11.7 cm from the exit window and the tank was filled with emulsion Code G are plotted in Figure 13. The measured beam radii (half power point) for these curves are listed in Table VI and plotted in Figure 14 along with the theoretical line  $r_c = 0.78 b g^{-0.7} \tau^{0.93}$  from Eq.(6).

## V. Discussion

A casual examination of Figure 7 shows quite reasonable agreement between the theoretical values of the delay and those measured in the scattering experiments on the diiodomethane/water emulsions Codes B, C and D. There is some discrepancy at optical thicknesses less than about 20, but at small optical thickness the probable error is of the order of  $\pm 10$  ps and as illustrated by the error bars the disagreement is not excessive. All the data from emulsion Code A, however, falls somewhat below and parallel to the 1.94 power law line, a fact which has defied rational explanation. These measurements were made with linearly polarized incident pulses but the detection system was not polarization sensitive and no effect should result.

The pulse stretching data for the diiodomethane emulsions displayed in Figure 9 shows behavior similar to the corresponding delay measurements. The increased scatter is due to the inherently poorer accuracy of the second moment calculations and the greater weight accorded to the tail of the scattered pulse. The fall off of the data points below the theoretical line at large optical thickness may be due to two factors. First, the duration of the scattered pulses is in some cases so great that the entire event could not be captured within the time-scale range of the streak camera. Those events in which the tail of the scattered pulse is known to be lost are identified in the tables by a dagger. Second, the single scatter albedo calculated for the

diiodomethane emulsions is less than 0.9997 and at long path, large optical thickness absorption of the scattered light may reduce the measured pulse stretching and delay.

On the other hand there is poor agreement between the theoretical delay and stretching and the measured values for the paraffin oil/water emulsions (Codes E, F, and G) as illustrated in Figures 8 and 10. The experimental data all falls considerably below the theoretical lines and moreover the functional dependence on optical thickness does not appear to be a simple power law. In particular the experimental delay data seem to indicate a very slow initial increase with optical thickness on the order of  $\tau^{0.3}$  for  $\tau \leq 20$  and a faster rise approximately proportional to  $\tau^{2.6}$  for  $\tau \geq 30$ . The one scattering parameter which is significantly different for the two types of emulsion is the asymmetry factor  $g = 1 - \langle \cos \theta \rangle$  which is as large as 0.17140 for the DIM emulsions and as small as 0.05045 for the oil emulsions. It is likely that the simple dependence on  $g$  assumed here is inadequate and that higher moments of  $\cos \theta$  must be included to describe multiple scattering in systems with very strong forward scattering,  $g \rightarrow 0$ . It is worth noting that there is more satisfactory agreement for the diiodomethane emulsions which exhibit the same degree of forward scattering as water droplets.

The effect on the delay and stretching caused by a reduced

field of view is illustrated in Figures 8 and 10 by the triangular data points. These measurements were made on emulsion Code G and should therefore be compared most closely with the diamond shaped data points at the same optical thickness. A dramatic decrease in the measured delay and stretching is evident. The delay is reduced by a factor of 4 and the stretching by a factor of 5 at an optical thickness of 73.

The variation of the integrated intensity of the scattered radiation with optical thickness displayed in Figures 11 and 12 does show the functional form predicted,  $I_{\tau}/I_0 \propto (g\tau + 1.42)^{-1}$ . However, the constant of proportionality is  $10^4$  times smaller than expected if the detector were located at the surface of the exit window. In these experiments the streak camera entrance slit was located 20 cm from the glass exit window a fact which may account in part for this difference.<sup>9</sup> The integrated intensity measurements were the least accurate of any made during these experiments but are certainly correct to within a factor of 2, i.e.,  $\pm 0.3$  on the logarithmic scale.

The effect of the reduced field of view on the received intensity is clear (triangles in Figure 12). The data falls off more rapidly with increasing optical thickness as would be expected from the fact that less of the light scattered through extreme angles is accepted. The down turn in the intensity data

for emulsion Code A evident at very large optical thicknesses in Figure 11 is probably another manifestation of the effects of the reduced albedo of this large droplet diiodomethane emulsion.

The irradiance profiles shown in Figure 13 are similar to the predicted shape.<sup>2</sup> The measured half power beam radii, Table VI and Figure 14, are however much smaller than the  $0.78 b g^{-0.07} \tau^{0.93}$  predicted, especially at small optical thickness. These measurements were made on the paraffin oil/water emulsion Code G and the discrepancy can again be attributed to the extremely strong forward scattering,  $g = 0.05045$ , which results from droplets with large size parameters and small relative index of refraction.

A perfunctory study of the shape of the scattered pulses has been made. First an attempt was made to fit the functional form of a gamma distribution, Eq.(10a), to the scattered pulse shape. The goodness of fit was so poor however that this was abandoned and the two gamma distribution form, Eq.(10b), currently in vogue,<sup>6</sup> was tried. This too yielded poor fits to pulses scattered by optically thin systems and only moderately good fits to long path, optically thick data as illustrated in Figures 15 and 16. These are least squares fits of the 2 gamma form to data obtained from the experiments on the diiodomethane emulsion Code A

and the paraffin oil emulsion Code G at optical thicknesses  $\tau = 167$  and  $\tau = 107$  respectively.

The relatively poor agreement between the theoretical and observed pulse shapes indicates that not much is to be gained by using the fitted curve to calculate the delay or stretching except in those cases where the tail of the scattered pulse extended beyond the range of the streak camera time scale. The equation of the theoretical curve in Figure 15 is  $I(t) = 0.94 t \exp(-1.94 t) + 0.27 t \exp(-0.60 t)$ ,  $t$  in nanoseconds. Twice the rms width of this pulse,  $2 \sigma_t = 4.60$  ns. This is to be compared to the directly calculated value of 1.74 ns (see Table IV A). When this is normalized by multiplying by  $c b^{-1} g^{-0.81}/1.28$ , with  $b$  and  $g$  appropriate to emulsion Code A, one gets 7800 for the normalized stretching which when plotted as the solid square datum on Figure 9 is still somewhat below the theoretical line for that optical thickness. It is however much closer than the corresponding hollow square.

The principal conclusion which can be drawn from this work is that there is reasonable agreement between the Monte Carlo simulation results and these experiments for the diiodomethane/water systems. Since these systems mimic water droplet clouds the application of the theory to scattering in clouds and fogs is certainly in order. The paraffin oil/water results on the other hand indicate that the present theory is inadequate for systems exhibiting extreme forward scatter and a

more complete theory is needed perhaps involving higher moments<sup>9</sup> of the scattering function,  $\langle \cos^2 \theta \rangle$ , etc.

There is of course much work which must be done before the whole story of the effects of multiple scattering on optical pulse propagation is known. A wider range of index of refraction should be explored as well as an expanded range of size parameters. The effects of the field of view of the receiver needs to be thoroughly studied as does the temporal behavior of polarized and depolarized scattered radiation when the incident pulse is linearly polarized. A complete pulse shape study would also provide a valuable addition to the understanding of multiple scattering.

#### ACKNOWLEDGEMENTS

This work was supported by Office of Naval Research and by National Science Foundation under Equipment Grant No. ENG 78-10526.

The author wishes to thank P. G. Rickman and B. K. Froemke for the many hours expended in constructing apparatus, producing emulsions, counting and sizing droplet distributions and collecting scattering data.

### References

1. E. A. Bucher and R. M. Lerner, Appl. Opt. 12, 2401 (1973).
2. E. A. Bucher, Appl. Opt. 12, 2391 (1973).
3. G. C. Mooradian, M. Geller, L. B. Stotts, D. H. Stephens and R. A. Krautwald, Appl. Opt. 18, 429 (1979).
4. G. R. Hostetter, "Downlink Laser Cloud Experiment, final Report," GTE/Sylvania, Contract N00014-78-C-0716 (Feb. 1980).
5. J. C. Matter and R. G. Bradley, Appl. Opt. 20, 2220 (1981).
6. G. C. Mooradian and M. Geller, Appl. Opt. 21, 1572 (1982).
7. A. Ishimaru, Proc. IEEE 65, 1030 (1977).
8. A. Ishimaru, J. Opt. Soc. Am. 68, 1045 (1978).
9. A. P. Cierro, "Multiple Scattering in Clouds," Pacific Sierra Research Corp., Report 923, Contract N00014-78-C0751 (Sept. 1979).
10. A. Zardecki and W. G. Tam, Appl. Opt. 19, 3782 (1980).
11. S. Ito and K. Furutsu, J. Opt. Soc. Am. 70, 366 (1980).
12. H. M. Gupta, Opt. Quantum Electron. 12, 499 (1980).
13. S. Ito, Appl. Opt. 20, 2706 (1981).
14. A. Ishimaru, Opt. Eng. 20, 63 (1981).
15. W. G. Tam, J. Opt. Soc. Am. 72, 1311 (1982).
16. S. R. Pal and A. I. Carswell, Appl. Opt. 15, 1990 (1976).
17. J. S. Ryan and A. I. Carswell, J. Opt. Soc. Am. 68, 900 (1978).
18. S. R. Pal and A. I. Carswell, Appl. Opt. 17, 2321 (1978).
19. J. S. Ryan, S. R. Pal and A. I. Carswell, J. Opt. Soc. Am. 69, 60 (1979).

20. A. Ishimaru, Y. Kuga, R. L.-T. Cheung, and K. Shimizu, J.

Opt. Soc. Am. 73, 131 (1983).

TABLE I

	<u>Paraffin Oil</u>	<u>Diiodomethane</u>
Density	0.8755	3.325
Index of Refraction	1.4628	1.738
Index Relative to Water	1.0974	1.304
Absorption Coefficient @ 532 nm	$\leq 4 \times 10^{-4} \text{ cm}^{-1}$	$2.4 \text{ cm}^{-1}$
Drift Velocity of 10 $\mu\text{m}$ Droplet in water	$2.44 \text{ cm hr}^{-1}$	$-45.6 \text{ cm hr}^{-1}$

TABLE II  
EMULSION PROPERTIES

Emulsion Code and Type	Mean Diameter ( $\mu\text{m}$ )	Standard Deviation ( $\mu\text{m}$ )	Number Density ( $\text{m}^{-3}$ )	Volume Fraction (percent)
A-DIM	8.27	4.69	$5.05 \times 10^{12}$	0.32
B-DIM	3.38	1.64	$1.06 \times 10^{14}$	0.37
C-DIM	3.88	2.46	$8.17 \times 10^{12}$	0.062
D-DIM	7.94	3.94	$1.70 \times 10^{13}$	0.80
E-OIL	1.86	0.85	$8.77 \times 10^{13}$	0.051
F-OIL	9.39	1.69	$3.00 \times 10^{12}$	0.14
G-OIL	12.93	3.77	$3.08 \times 10^{12}$	0.42

TABLE III  
SCATTERING PARAMETERS

Emulsion Code	Size Parameter $\pi\langle d \rangle / \lambda$	Mean Scatter Cross Section $\sigma_s (\mu\text{m})^2$	Scattering Length $b (\text{mm})$	Asymmetry Factor $g = 1 - \langle \cos\theta \rangle$	Single Scatter Albedo
A	65.1*	148	1.34	0.14315	0.99926
B	26.6	24.2	0.389	0.17073	0.99970
C	30.5	36.0	3.40	0.17140	0.99964
D	62.5	130	0.453	0.14177	0.99926
E	14.6	8.95	1.27	0.07788	1.00000
F	73.9	152	2.19	0.06075	1.00000
G	101.8	298	1.09	0.05045	1.00000

\* Wavelength in medium (water)  $\lambda = 0.532/1.333 = 0.399 \mu\text{m}$

TABLE IVA

Path Length Z (cm)	Optical Thickness $\tau$	Delay $\Delta t$ (ps)	Stretching $2 \sigma_t$ (ps)	Relative Intensity
1.2	18	23	5	$4.9 \times 10^{-5}$
2.2	33	24	42	$4.3 \times 10^{-5}$
3.2	48	114	250	$1.5 \times 10^{-5}$
4.2	63	260	440	$1.3 \times 10^{-5}$
5.2	78	400	600	$1.1 \times 10^{-5}$
6.2	93	600	930	$1.0 \times 10^{-5}$
7.2	108	930	1330	$1.0 \times 10^{-5}$
8.2	123	1170	1580	$8.1 \times 10^{-6}$
9.2	138	1320	1630	$6.9 \times 10^{-6}$
10.2	153	1320 <sup>†</sup>	1790 <sup>†</sup>	$5.6 \times 10^{-6}$
11.2	167	1440 <sup>†</sup>	1740 <sup>†</sup>	$4.6 \times 10^{-6}$

TABLE IVB

Path Length Z (cm)	Optical Thickness $\tau$	Delay $\Delta t$ (ps)	Stretching $2 \sigma$ (ps)	Relative Intensity
0.5	13	10	13	$1.9 \times 10^{-4}$
1.0	26	86	170	$4.8 \times 10^{-5}$
1.5	39	230	380	$3.7 \times 10^{-5}$
2.0	51	350	490	$3.1 \times 10^{-5}$
3.0	77	590	690	$4.7 \times 10^{-5}$
4.0	103	1250 <sup>†</sup>	590 <sup>†</sup>	$8.4 \times 10^{-6}$
6.0	154	1980 <sup>†</sup>	650 <sup>†</sup>	$2.8 \times 10^{-6}$

TABLE IVC

Path Length Z (cm)	Optical Thickness $\tau$	Delay $\Delta t$ (ps)	Stretching $2 \sigma$ (ps)	Relative Intensity
2.0	6	68	14	$1.2 \times 10^{-2}$
4.0	12	77	22	$1.5 \times 10^{-4}$
6.0	18	132	190	$5.9 \times 10^{-5}$
8.0	24	290	510	$3.8 \times 10^{-5}$
11.7	34	720	1180	$2.5 \times 10^{-5}$

TABLE IVD

Path Length Z (cm)	Optical Thickness $\tau$	Delay $\Delta t$ (ps)	Stretching $2 \sigma$ (ps) <sup>†</sup>	Relative Intensity
0.5	11	0	11	$1.7 \times 10^{-4}$
1.0	22	70	150	$3.2 \times 10^{-5}$
2.0	44	250	430	$2.1 \times 10^{-5}$
3.0	66	530 <sup>†</sup>	380 <sup>†</sup>	$9.1 \times 10^{-6}$
4.0	88	750 <sup>†</sup>	470 <sup>†</sup>	$3.6 \times 10^{-6}$

TABLE IVE

Path Length Z (cm)	Optical Thickness $\tau$	Delay $\Delta t$ (ps)	Stretching $2 \sigma_z$ (ps)	Relative Intensity
0.5	4	2	4	$1.9 \times 10^{-2}$
1.0	8	12	11	$6.8 \times 10^{-4}$
2.0	16	25	19	$1.1 \times 10^{-4}$
4.0	32	39	46	$4.0 \times 10^{-5}$
6.0	47	114	180	$2.5 \times 10^{-5}$
8.0	63	220	310	$1.5 \times 10^{-5}$
10.0	79	420	570	$1.4 \times 10^{-5}$
11.7	92	740	1020	$1.4 \times 10^{-5}$

TABLE IVF

Path Length Z (cm)	Optical Thickness $\tau$	Delay $\Delta t$ (ps)	Stretching $2 \sigma$ (ps)	Relative Intensity
0.5	2	13	17	$1.5 \times 10^{-1}$
1.0	5	2	18	$3.6 \times 10^{-2}$
2.0	9	11	17	$1.8 \times 10^{-3}$
4.0	18	34	17	$8.9 \times 10^{-5}$
6.0	27	33	35	$4.5 \times 10^{-5}$
8.0	37	64	79	$3.1 \times 10^{-5}$
10.0	46	95	130	$1.9 \times 10^{-5}$
11.7	53	120	170	$1.1 \times 10^{-5}$

TABLE IVG

Path Length Z (cm)	Optical Thickness $\tau$	Delay $\Delta t$ (ps)	Stretching $2 \sigma$ (ps)	Relative Intensity
0.5	5	20	7	$2.0 \times 10^{-2}$
1.0	9	23	0	$2.1 \times 10^{-3}$
1.5	14	25	10	$6.5 \times 10^{-4}$
2.0	18	36	12	$3.0 \times 10^{-4}$
3.0	28	36	25	$1.4 \times 10^{-4}$
4.0	37	56	130	$1.3 \times 10^{-4}$
6.0	55	200	350	$4.4 \times 10^{-5}$
8.0	73	390	650	$4.4 \times 10^{-5}$
10.0	92	520	800	$1.7 \times 10^{-5}$
11.7	107	980 <sup>†</sup>	1600 <sup>†</sup>	$1.9 \times 10^{-5}$

TABLE V

Path Length Z (cm)	Optical Thickness $\tau$	Delay $\Delta t$ (ps)	Stretching $2 \sigma_t$ (ps)	Relative Intensity
2.0	18	3	18	$2.0 \times 10^{-4}$
4.0	37	6	25	$4.1 \times 10^{-5}$
6.0	55	26	53	$1.8 \times 10^{-5}$
8.0	73	100	130	$6.2 \times 10^{-6}$

TABLE VI

Path Length (cm)	Optical Thickness $\tau$	Beam Radius (cm)
1.0	9	0.2
4.0	37	19
6.0	55	30
8.0	73	44
11.7	107	68

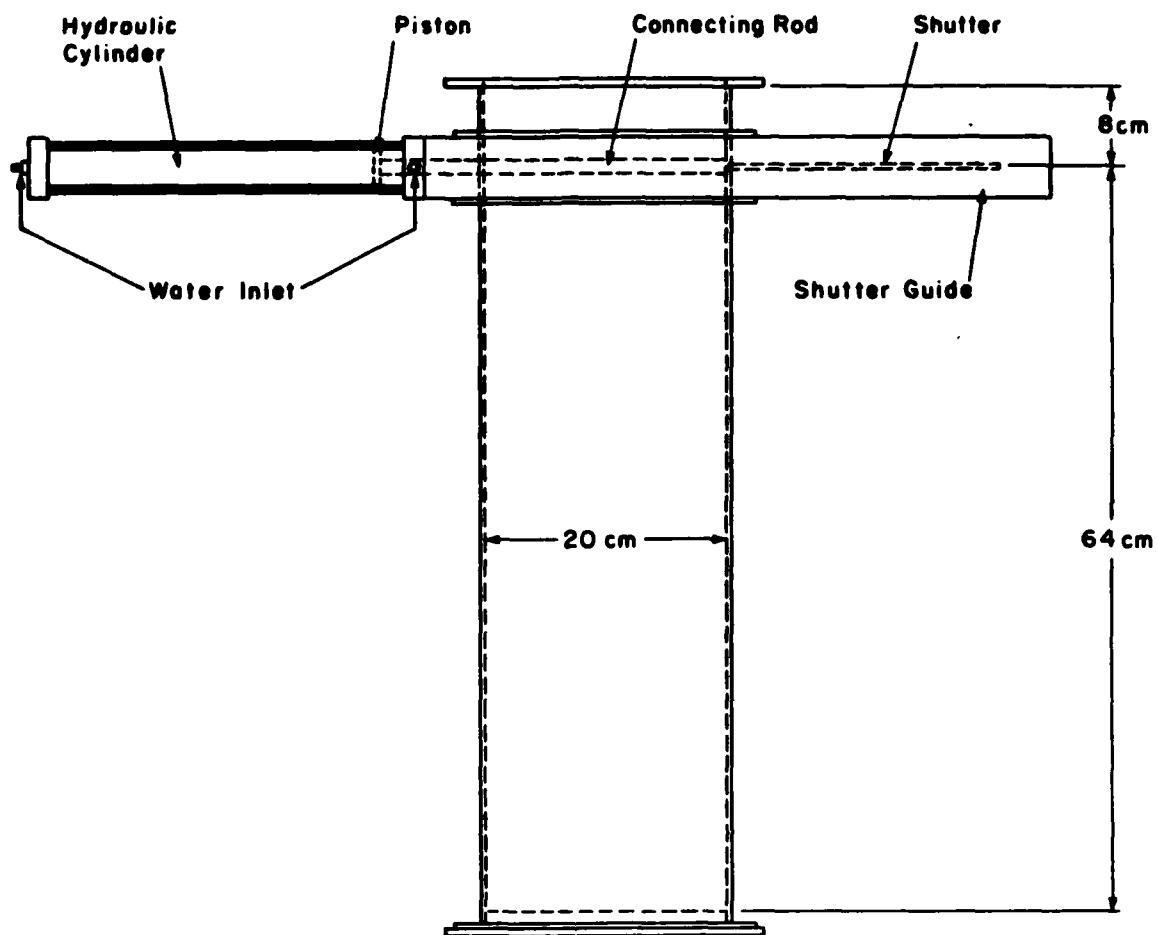


Figure 1. Apparatus for separating large and small buoyant droplets in, e.g., an oil/water emulsion. A thin stainless steel shutter may be drawn across the column to isolate the top 1/9 of the volume from the bottom 8/9. For diiodomethane/water or other emulsions with droplets more dense than the bulk medium the column is inverted with the shutter located near the bottom.

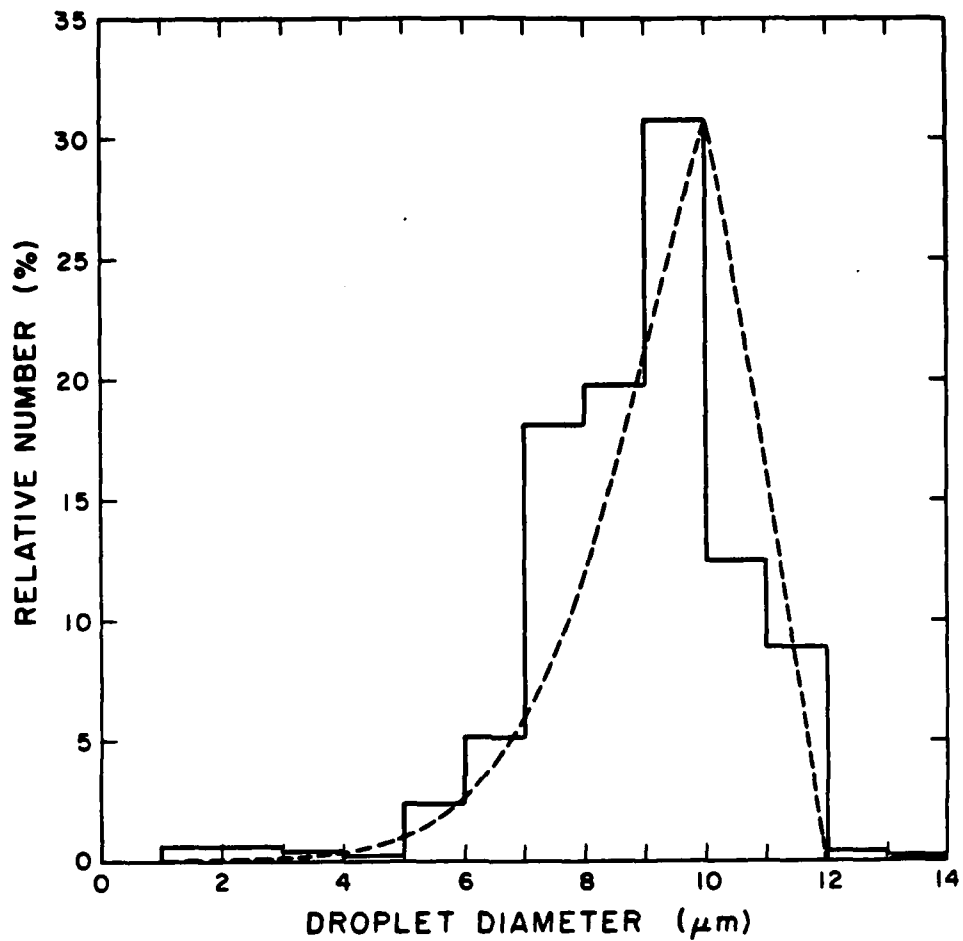


Figure 2. Size distribution histogram for emulsion Code F. The dashed line is the theoretical distribution according to Eq. 16. The measured mean diameter and standard deviation are 9.39 μm and 1.69 μm compared to the predicted values of 9.32 μm and 1.30 μm respectively. A total of 802 droplet diameters were measured on 400X micrographs of samples of the emulsion.

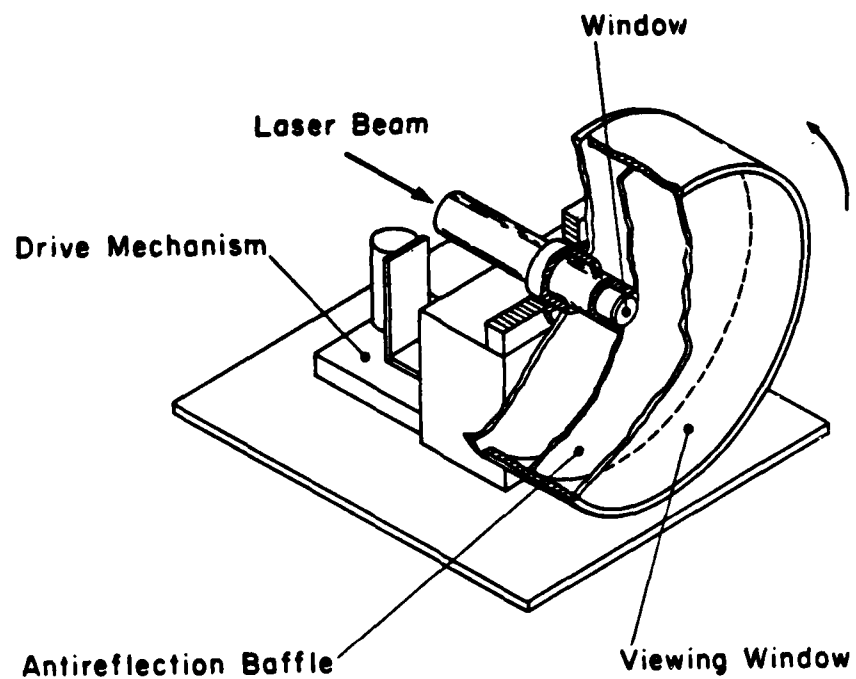


Figure 3. Scattering cell. The cylinder rotates at a constant speed of 1 rpm to prevent the emulsion droplets from collecting at the top or bottom. The distance between the entrance and exit windows is variable between 0.2 cm and 11.7 cm. All interior surfaces are flat black to reduce reflection of escaping radiation back into the scattering medium.

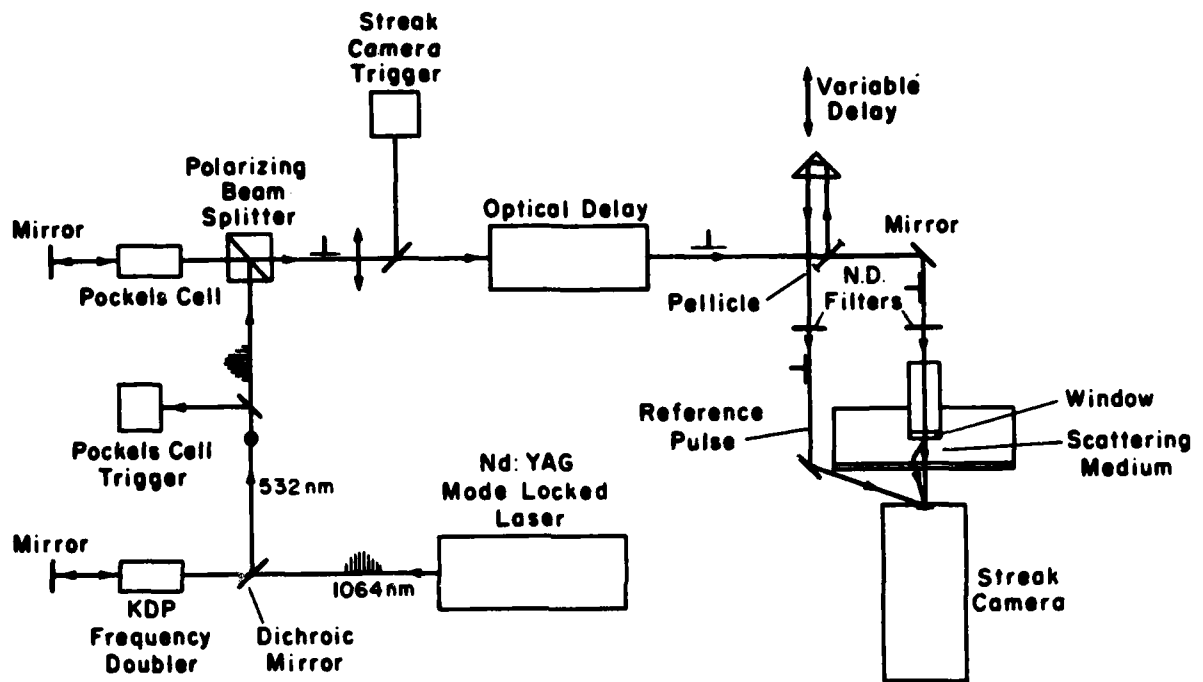


Figure 4. Schematic layout of the optical system.

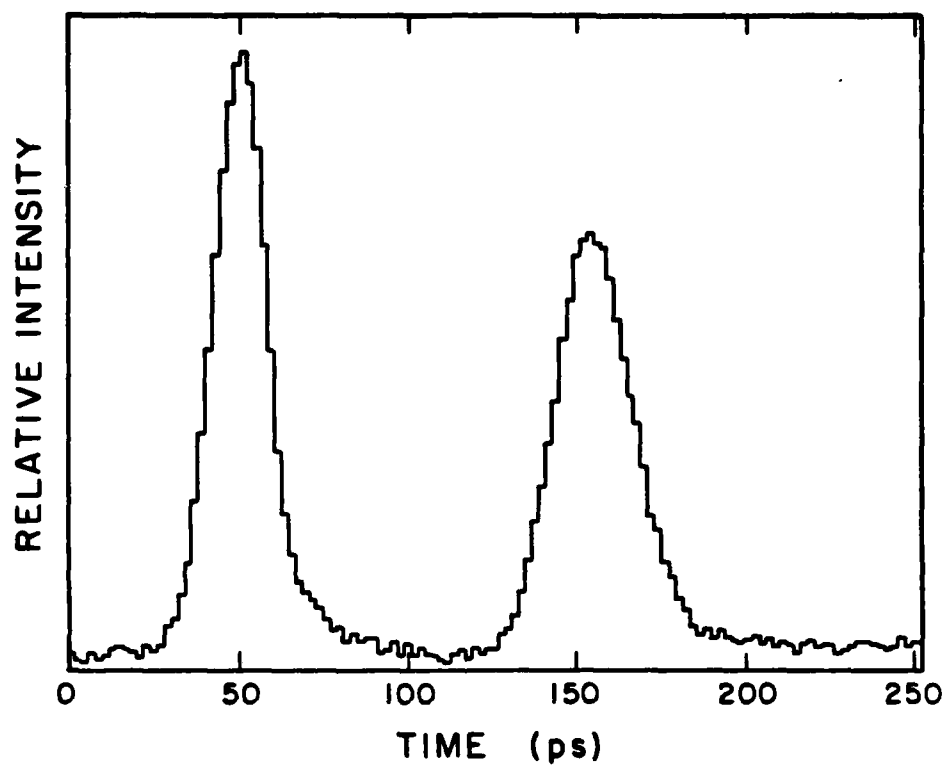


Figure 5. Typical intensity versus time streak camera record. The left hand pulse is the reference and the right hand the pulse which has passed through the scattering medium. Optical thickness  $\tau = 9$ , emulsion Code A.

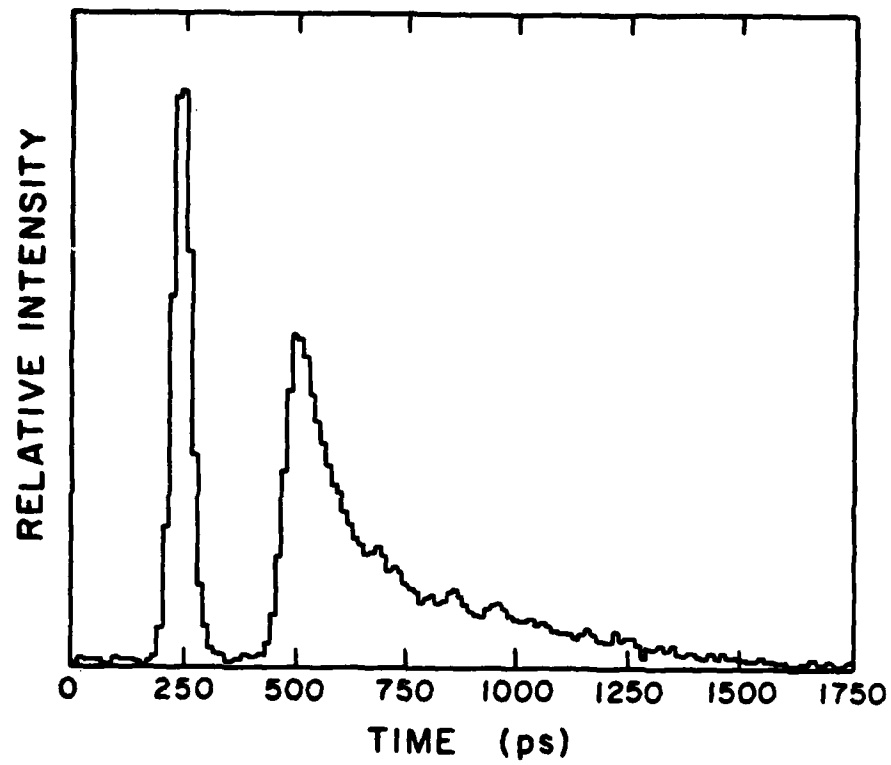


Figure 6. The same as Figure 5 except  $\tau = 63$ .

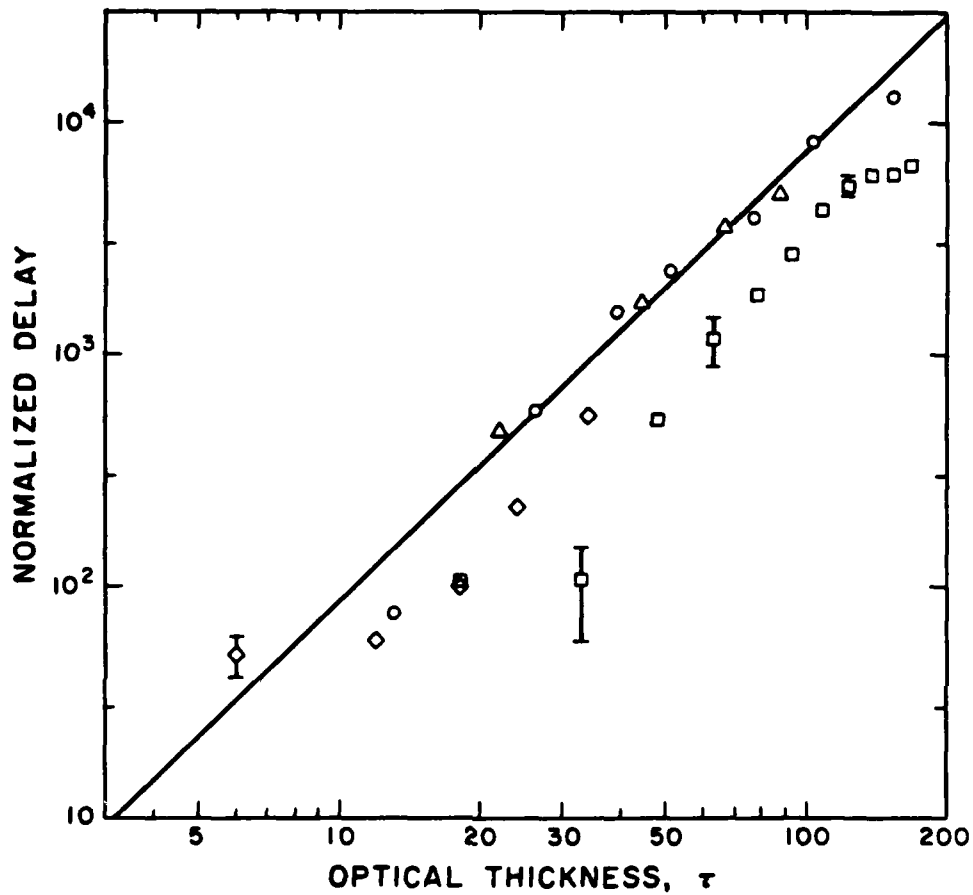


Figure 7. Delay in the mean arrival time due to multiple scattering versus optical thickness for diiodomethane emulsions. Measured delay times have been normalized by multiplying by  $c b^{-1} g^{-0.94}/0.62$ .  $\square$  - code A;  $\circ$  - code B;  $\diamond$  - code C; and  $\Delta$  - code D. The line is  $\tau^{1.94}$ .

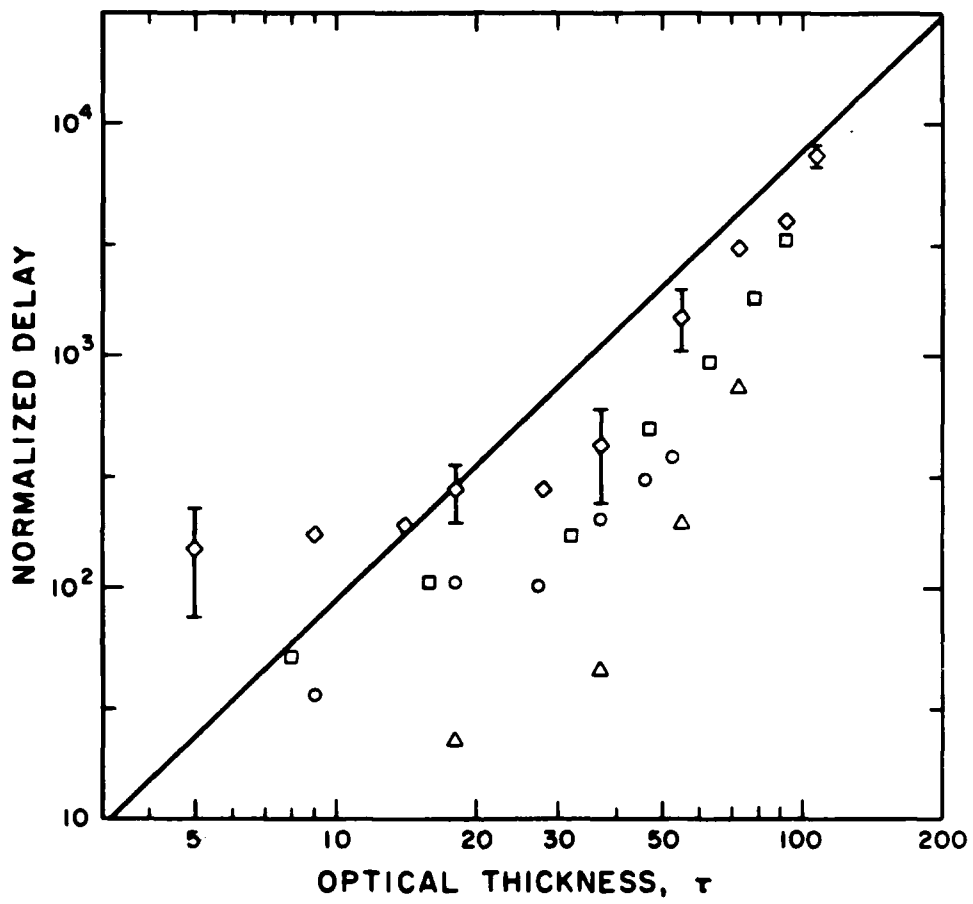


Figure 8. The same as Figure 7 but for paraffin oil emulsions.

□ - code E; ○ - code F; ◇ - code G; and Δ - code G with restricted field of view (16°) detector.

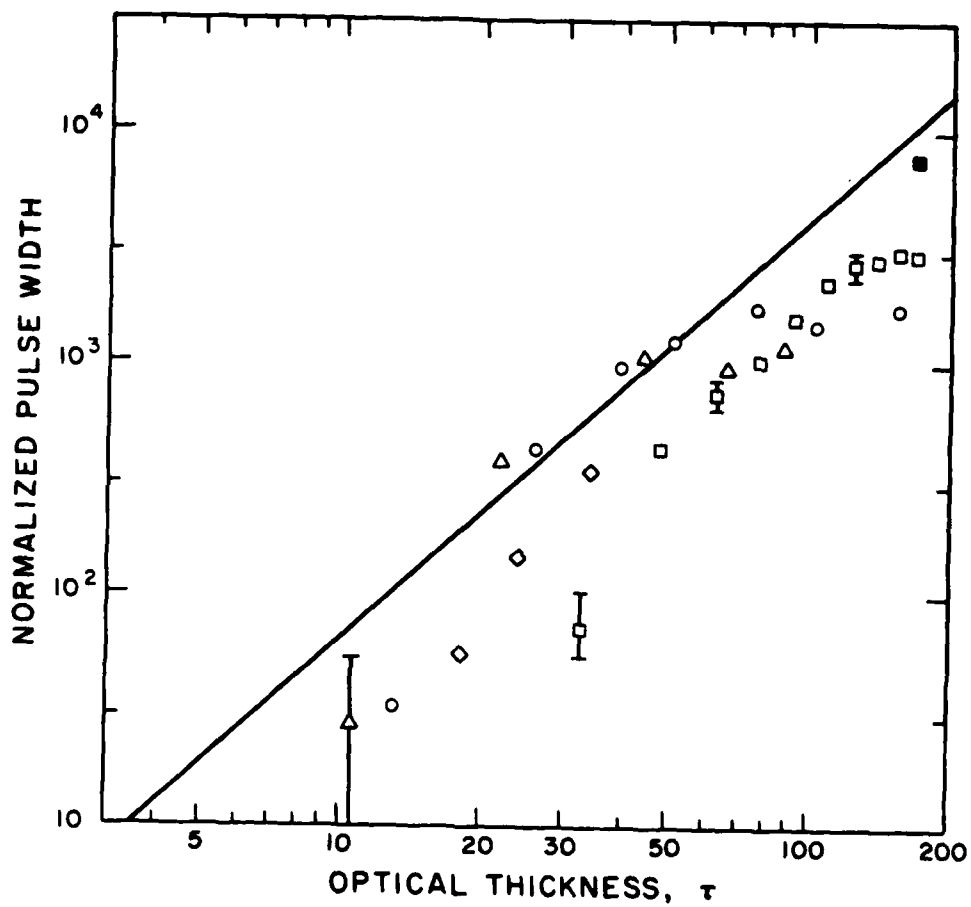


Figure 9. Pulse stretching normalized by multiplication by  $c b^{-1} g^{-0.81}/1.28$  versus optical thickness for diiodomethane emulsions.  $\square$  - code A;  $\circ$  - code B;  $\diamond$  - code C; and  $\Delta$  - code D. The line is  $\tau^{1.81}$ .

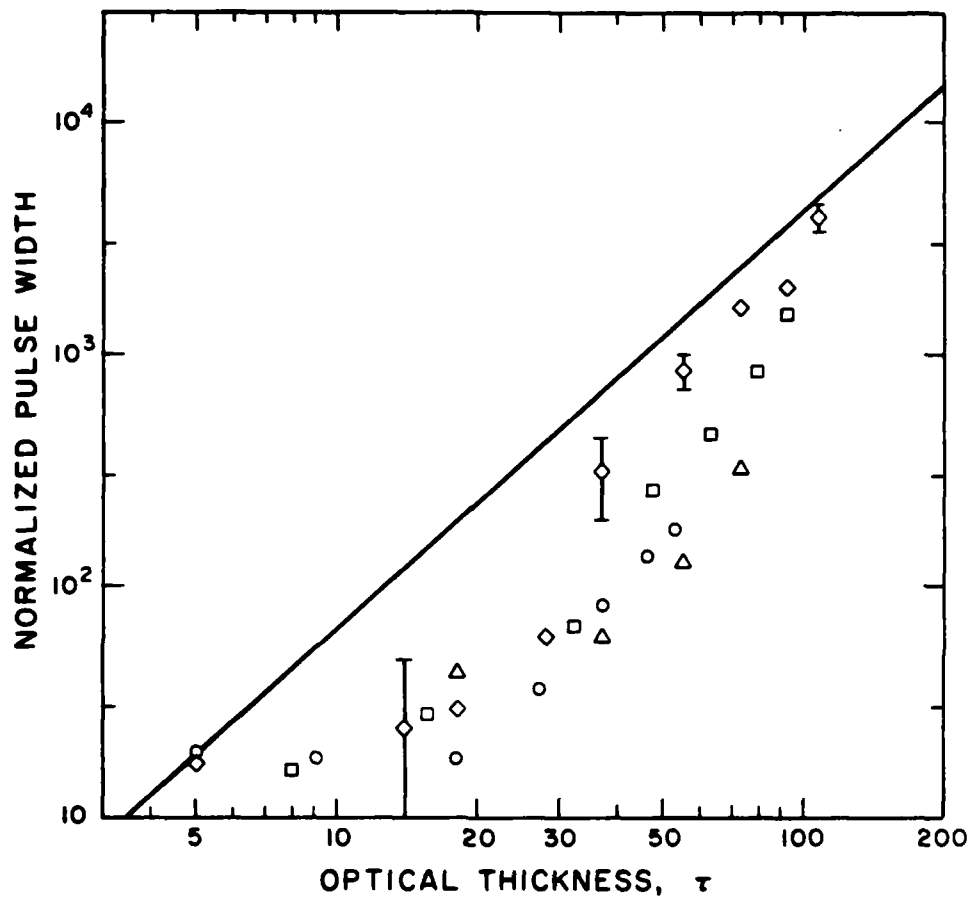


Figure 10. The same as Figure 9 but for paraffin oil emulsions.

□ - code E; ○ - code F; ◇ - code G; and Δ - code G with restricted field of view (16°) detector.

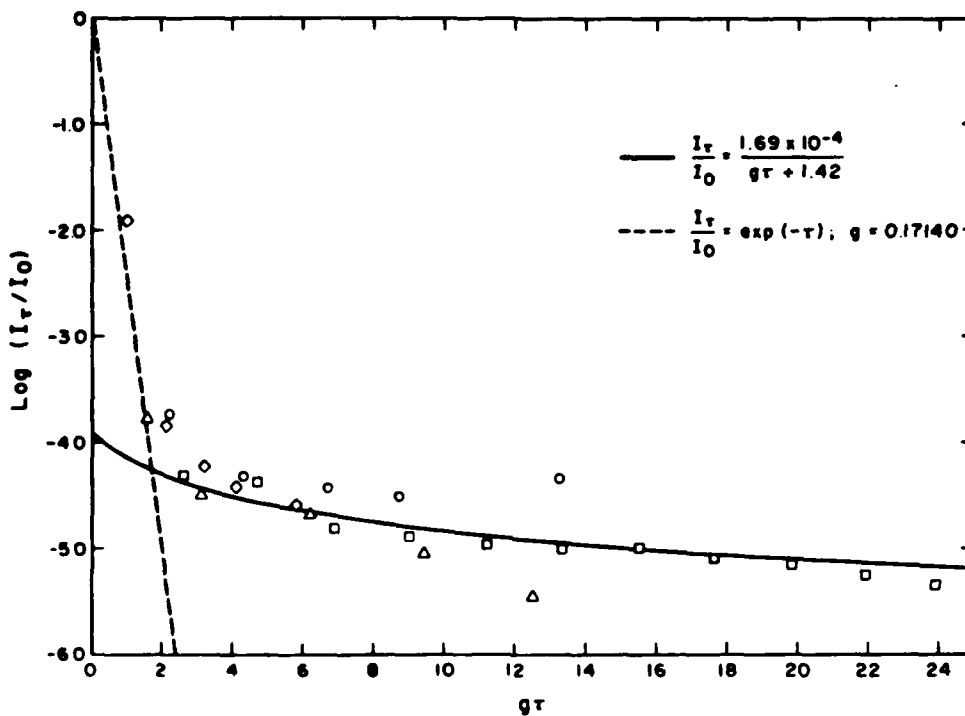


Figure 11. Logarithm of the relative integrated intensity of scattered pulses versus optical thickness times the asymmetry factor,  $g\tau$ , for diiodomethane emulsions.

□ - code A; ○ - code B; ◇ - code C; and △ - code D.

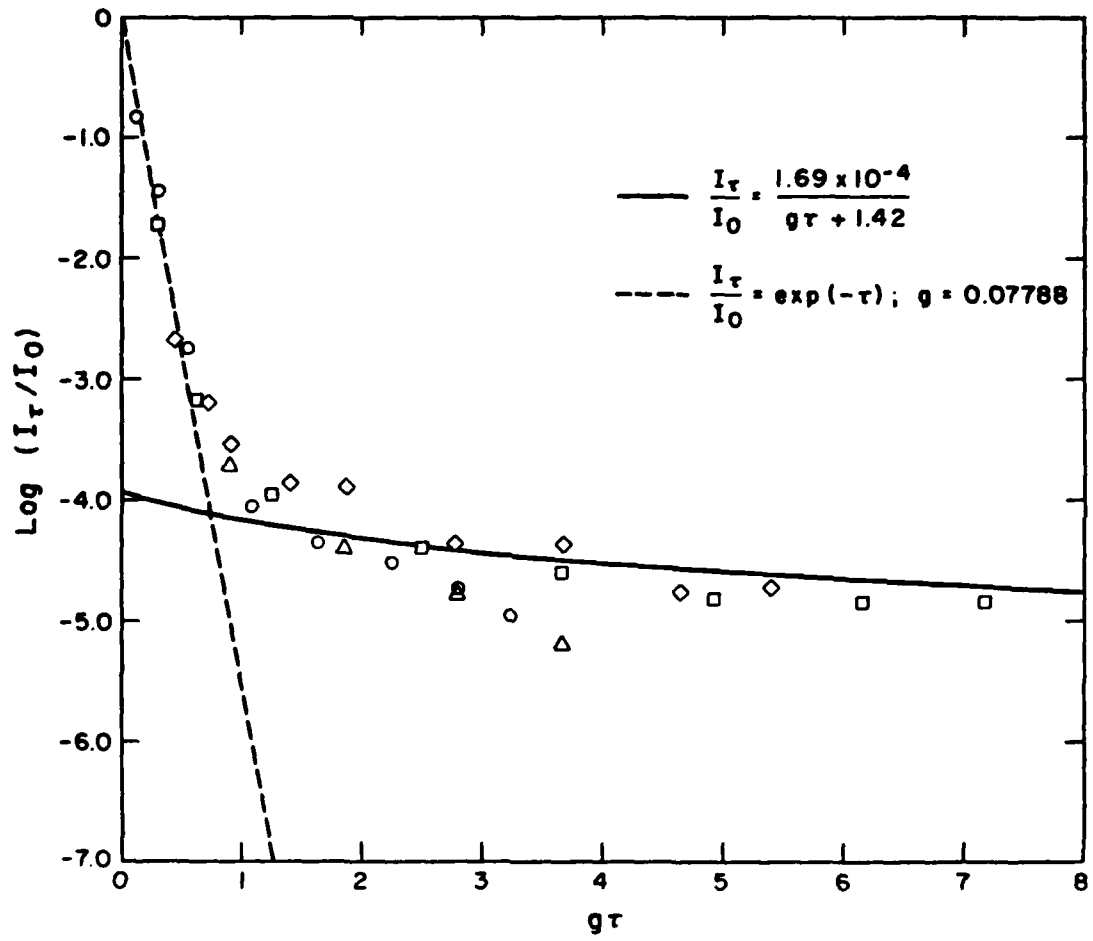


Figure 12. The same as Figure 11 but for paraffin oil emulsions.

□ - code E; ○ - code F; ◇ - code G; and △ - code G  
with restricted field of view (16°) detector.

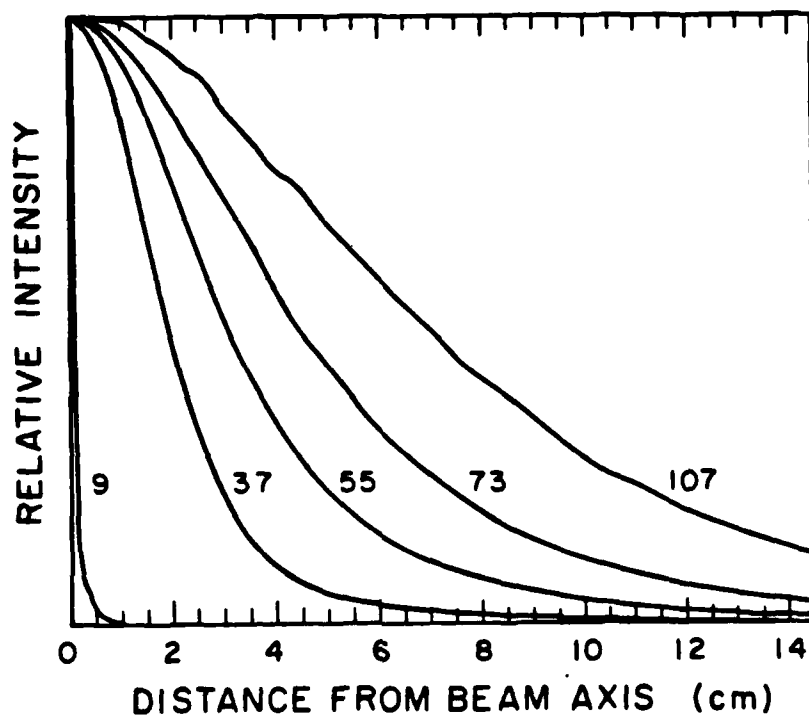


Figure 13. Profiles of the irradiance at the exit window of the scattering cell for the optical thicknesses indicated on the curves. Paraffin oil emulsion code G.

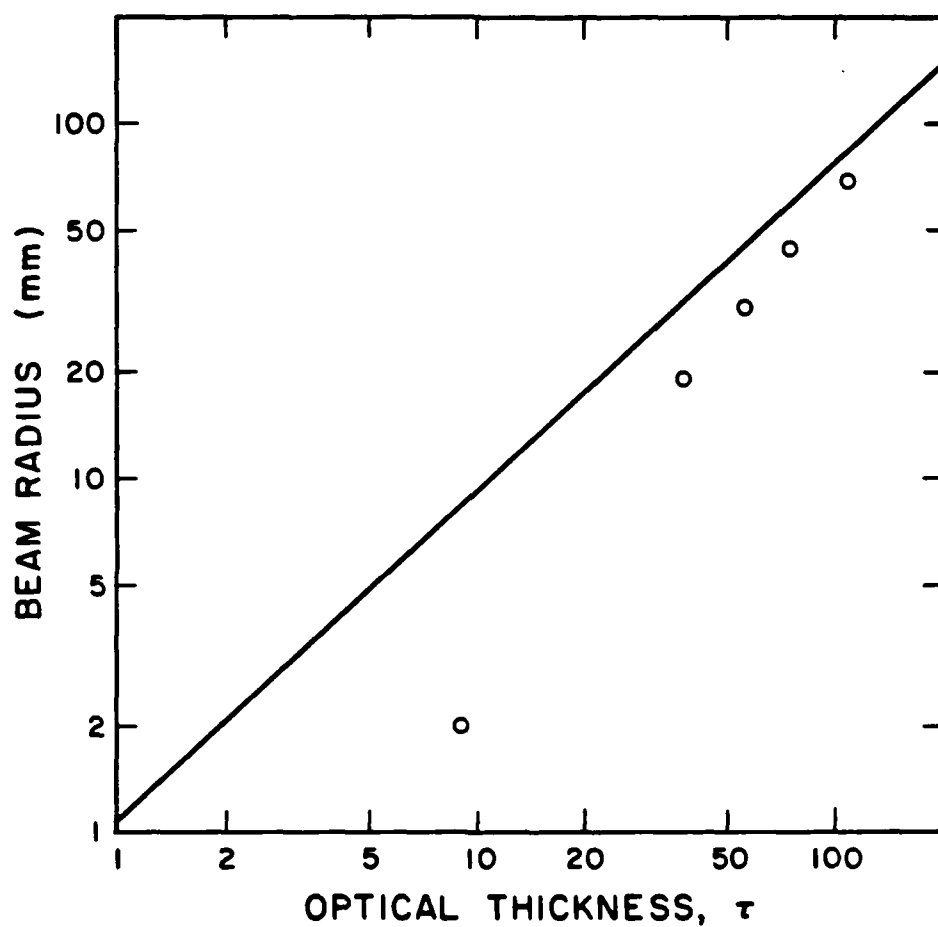


Figure 14. Beam radius versus optical thickness as measured from the half power points on the profiles displayed in Figure 13. The line is  $r = 0.78 b g^{-0.7} \tau^{0.93}$ .

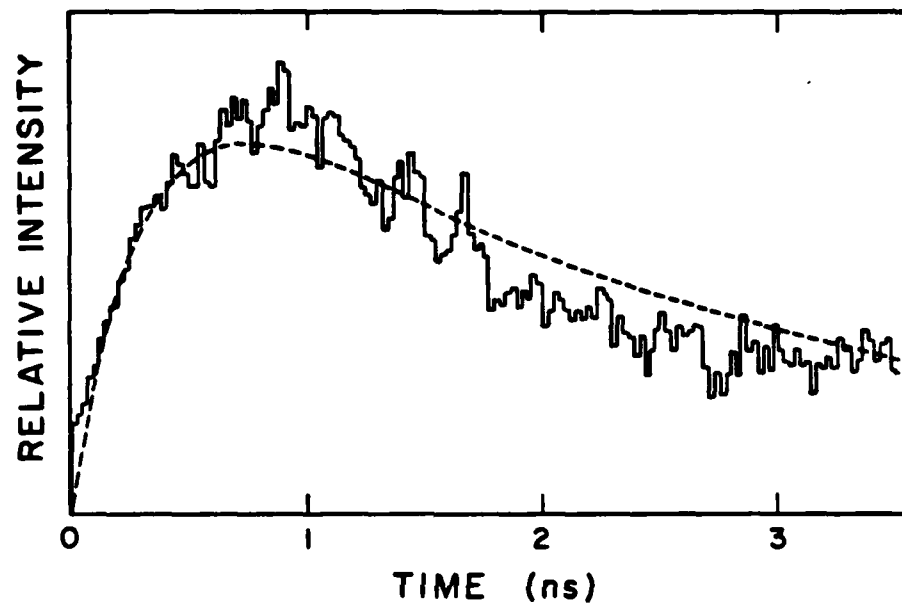


Figure 15. Least squares fit of two gamma distribution functional form to pulse scattered by 167 optical thicknesses of diiodomethane emulsion code A. -----  $0.94 t \exp(-1.94 t) + 0.27 t \exp(-0.60 t)$ ,  $t$  in nanoseconds.

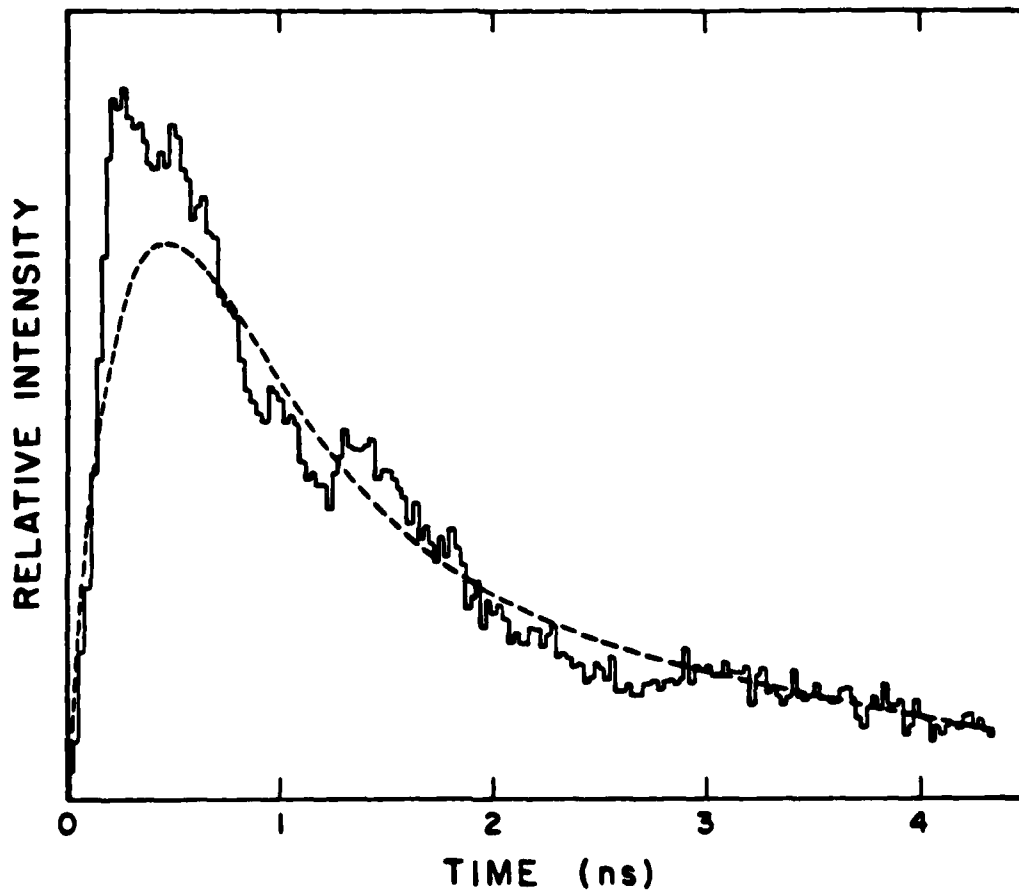


Figure 16. The same as Figure 15 but for a pulse scattered by 107 optical thicknesses of paraffin oil emulsion code G.  
 -----  $3.28 t \exp(-2.78 t) + 0.34 t \exp(-0.77 t)$ ,  $t$  in nanoseconds.

4-  
DT